AGU PUBLICATIONS

JGR

Journal of Geophysical Research: Atmospheres

RESEARCH ARTICLE
10.1002/2015JD023998

This article is a companion to *Matsui* [2016] doi:10.1002/2015JD023999.

Key Points:
- The simulations reveal a large uncertainty of BC radiative effects due to the treatment of emissions
- BC radiative effects are 3–5 times more sensitive to emission parameters than BC mass concentrations
- The results show the importance of resolving BC mixing state and absorption enhancement in models

Correspondence to:
H. Matsui,
matsui@nagoya-u.jp

Citation:
Matsui, H. (2016), Black carbon simulations using a size- and mixing-state-resolved three-dimensional model: 1. Radiative effects and their uncertainties, *J. Geophys. Res. Atmos.*, *121*, 1793–1807, doi:10.1002/2015JD023998.

Received 27 JUL 2015
Accepted 25 DEC 2015
Accepted article online 3 JAN 2016
Published online 20 FEB 2016

Black carbon simulations using a size- and mixing-state-resolved three-dimensional model: 1. Radiative effects and their uncertainties

H. Matsui[1,2,3]

[1]Graduate School of Environmental Studies, Nagoya University, Nagoya, Japan, [2]Department of Earth and Atmospheric Sciences, Cornell University, Ithaca, New York, USA, [3]Department of Environmental Geochemical Cycle Research, Japan Agency for Marine-Earth Science and Technology, Yokohama, Japan

Abstract This study quantifies how uncertainties in the size distribution and mixing state parameters of black carbon (BC) emissions translate into the uncertainties in BC radiative effects by using a particle-size- and mixing-state-resolved three-dimensional model, the Weather Research and Forecasting model with chemistry (WRF-chem) with the Aerosol Two-dimensional bin module for foRmation and Aging Simulation (ATRAS) and the Model for Simulating Aerosol Interactions and Chemistry (MOSAIC). The WRF-chem/ATRAS-MOSAIC model can explicitly calculate BC processes in the atmosphere, such as BC aging due to condensation and coagulation and the resulting enhancement of absorption and cloud condensation nuclei activity, with 12 size and 10 BC mixing state bins (128 bins in total). Fifteen model simulations perturbing the emission parameters within their uncertainties are conducted over East Asia (spring 2009) to understand which parameters and processes are important and which are associated with the uncertainty in evaluating BC radiative effects. The simulations reveal a large variability (uncertainty) of BC optical and radiative variables over the East Asian region (the variability is 58–99%), which corresponds to ranges of BC radiative effect of 1.6–2.8 W m^{-2} at the top of the atmosphere and from −5.2 to −2.1 W m^{-2} at the surface over East Asia. BC optical and radiative variables are 3 to 5 times sensitive to the size and the mixing state in emissions than BC mass concentrations (the variability is 20%). The two main causes of the difference in sensitivity are the reduction of the variability of BC mass concentrations by coagulation and the enhancement of the variability of BC absorption by resolving BC mixing state. These complicated responses of aerosol processes can be calculated for the first time using a detailed aerosol model such as ATRAS. The results suggest that the following two points are important in the estimation of BC radiative effects: (1) reduction of the uncertainties in the aerosol size distribution and mixing state in emissions and (2) improvement of the representation of BC mixing state and absorption enhancement in aerosol models because most models do not treat them sufficiently.

1. Introduction

Black carbon (BC) aerosols in the atmosphere play an important role in Earth's climate system because they efficiently absorb solar radiation and heat the atmosphere [*Ramanathan et al.*, 2001; *Ramanathan and Carmichael*, 2008; *Bond et al.*, 2013; *Boucher et al.*, 2013]. BC particles are emitted from the incomplete combustion of fossil fuels, biomass, and biofuels [*Streets et al.*, 2003; *Bond et al.*, 2004, 2007], and many of these fresh BC particles are generally thinly coated and are hydrophobic. BC particles are gradually coated by inorganic and organic species and become hydrophilic through aging processes (condensation, coagulation, and photochemical oxidation) during transport [*Moteki et al.*, 2007]. Hydrophilic BC particles act as cloud condensation nuclei (CCN) and modify cloud microphysical properties [*Seinfeld and Pandis*, 2006; *Kuwata et al.*, 2009]. Aging processes enhance both absorption efficiency and CCN activity of BC particles. BC absorption efficiency is enhanced by the coating of scattering material, which acts as a lens and directs more photons to the BC core [*Bond et al.*, 2006]. The enhancement of absorption efficiency is estimated to be up to a factor of two and impacts aerosol optical and radiative parameters [*Jacobson*, 2000, 2001; *Bond et al.*, 2006, 2013; *Shiraiwa et al.*, 2008, 2010; *Oshima et al.*, 2009]. The enhancement of CCN activity increases the wet scavenging rate of BC and reduces the lifetime of BC [*Stier et al.*, 2006; *Oshima et al.*, 2009; *Riemer et al.*, 2010; *Zaveri et al.*, 2010].

The number concentration, particle size distribution, and BC mixing state are important parameters for representing aging processes and the resulting enhancement of absorption efficiency and CCN activity. However, few three-dimensional models can resolve these parameters sufficiently [*Jacobson*, 2002]. In most three-dimensional

models, the enhancement of CCN activity has been represented by parameterizations that calculate the conversion rate of BC from hydrophobic to hydrophilic by use of a constant aging timescale or a timescale dependent on some chemical species such as the hydroxyl radical and/or sulfuric acid [*Riemer et al.*, 2004; *Liu et al.*, 2011; *Oshima and Koike*, 2013]. These parameterizations have been used to calculate the lifetime and the removal rate of BC. In contrast, less attention has been paid to the enhancement of absorption efficiency. Few three-dimensional models sufficiently resolve the gradual enhancement of absorption efficiency by BC aging processes during transport. Models need to resolve the aging processes and the resulting diversity of BC mixing states in the atmosphere [*Matsui et al.*, 2013a] to calculate the enhancement of absorption efficiency accurately.

Matsui et al. [2014a] have developed an aerosol module designated the Aerosol Two-dimensional bin module for foRmation and Aging Simulation (ATRAS). The ATRAS module resolves both aerosol size (12 bins) and BC mixing state (10 bins); it represents number concentration, size distribution, and BC mixing state explicitly by considering BC aging (changes in BC size and mixing state by condensation and coagulation) [*Matsui et al.*, 2013a], organic aerosol formation [*Matsui et al.*, 2014b], and new particle formation processes [*Matsui et al.*, 2011, 2013b]. The module explicitly calculates the series of BC processes that occur in the atmosphere based on microphysical and chemical processes: emission, transformation by condensation and coagulation, enhancement of absorption efficiency and CCN activity by transformation, aerosol activation to cloud, and dry and wet deposition. The module can be used to understand which parameters and processes are important and which are associated with the greatest uncertainty in evaluating BC radiative effects.

This study evaluates the uncertainties of BC and its optical and radiative variables over East Asia (spring 2009) by using the ATRAS module. Though there are many uncertain BC parameters (e.g., mass flux of emissions, refractive index), this study focuses on the parameters of aerosol size distribution and mixing state in emissions because they are important for both microphysical processes and optical properties and their interactions. This study quantifies how uncertainties in the size distribution and mixing state parameters of BC emissions translate into the uncertainties in BC radiative effects by using the detailed aerosol module, ATRAS, which can adequately resolve both aerosol size and mixing state. The ATRAS module and the simulation setup used in this study are described in sections 2 and 3, respectively. In section 4, the results of the base case simulation (section 4.1), the variability of BC and its optical/radiative variables due to the uncertainty in the size distribution and mixing state in emissions (sections 4.2 and 4.3), and BC radiative effect and its uncertainty (section 4.4) are discussed.

2. Size- and Mixing-State-Resolved Model (WRF-Chem/ATRAS-MOSAIC)

The ATRAS module [*Matsui et al.*, 2014a] was developed using the framework of the Weather Research and Forecasting model with chemistry (WRF-chem) version 3.4 [*Grell et al.*, 2005; *Skamarock et al.*, 2008] in combination with the Model for Simulating Aerosol Interactions and Chemistry (MOSAIC) aerosol module [*Fast et al.*, 2006; *Zaveri et al.*, 2008].

Figure 1 shows the aerosol representation and processes considered in the ATRAS module. The module uses a two-dimensional bin representation for particles from 40 nm to 10 μm in dry diameter, with 12 size bins and 10 BC mixing state bins to resolve BC aging processes by condensation and coagulation. BC mixing state bins are defined in terms of the BC mass fraction, the ratio of the BC mass to the total aerosol mass under dry conditions: pure BC particles (BC mass fraction >0.99), eight internally mixed BC particles (BC mass fractions of 0.99–0.9, 0.9–0.8, 0.8–0.65, 0.65–0.5, 0.5–0.35, 0.35–0.2, 0.2–0.1, and 0.1–0), and BC-free particles (BC mass fraction = 0). The module also uses eight size bins for particles from 1 to 40 nm in diameter to calculate new particle formation processes. Aerosol particles in the aerosol phase and the cloud phase are treated separately, as shown in Figure 1. The module therefore uses 256 bins [$(12 \times 10 + 8) \times 2$ bins] in total to represent aerosol particles. Mass concentrations of sulfate, nitrate, ammonium, organics (primary + secondary), BC, dust, sodium, chloride, and aerosol water and number concentrations are traced in each aerosol bin.

The ATRAS module considers the following microphysical and chemical processes: emission, nucleation, condensation/evaporation of inorganic species, coagulation, organic aerosol formation, aerosol activation to cloud [*Abdul-Razzak and Ghan*, 2000], evaporation from cloud, aqueous-phase chemistry [*Fahey and Pandis*, 2001], dry deposition, and in-cloud and below-cloud scavenging [*Easter et al.*, 2004] (Figure 1). The nucleation rate at a particle size of 1 nm is calculated using the activation theory [*Kulmala et al.*, 2006] with a coefficient of $2 \times 10^{-7}\ s^{-1}$ based on *Matsui et al.* [2011, 2013b]. Condensation and evaporation of inorganic species are calculated for each aerosol bin by using the MOSAIC module [*Zaveri et al.*, 2005a, 2005b, 2008].

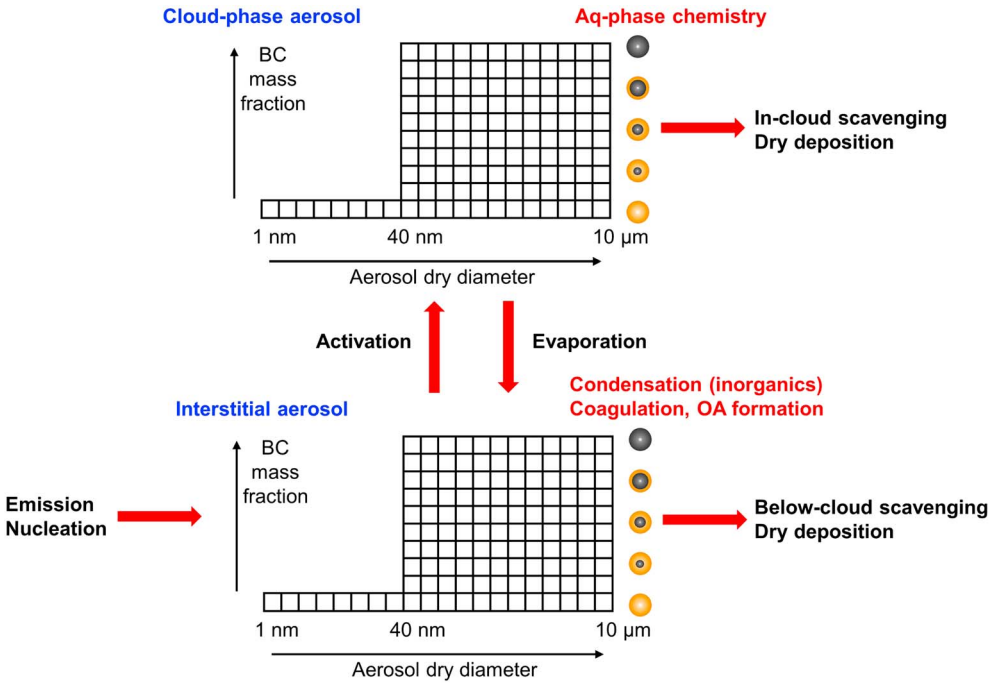

Figure 1. Schematic figure showing the aerosol bin representation adopted and the processes considered in the ATRAS module. BC-free particles with diameters of 1–40 nm (eight bins) are used to calculate new particle formation processes. For particles with diameters of 40 nm to 10 μm, 12 × 10 bins are used to resolve both aerosol size (dry condition) and BC mixing state. Interstitial and cloud-phase aerosols are treated separately in this module.

Coagulation within two-dimensional bins is calculated based on the scheme in *Matsui et al.* [2013a], which is an extension of the semi-implicit method of *Jacobson et al.* [1994]. Organic aerosol formation is calculated based on a volatility-basis set approach that represents 9 volatility classes using 53 surrogate vapor species and 53 corresponding aerosol species [*Matsui et al.*, 2014b]. Gas-phase chemistry is calculated by using SAPRC-99 [*Carter*, 2000] with a modification for precursor organic vapors [*Matsui et al.*, 2014b]. Photolysis is calculated with the Fast-J photolysis scheme [*Wild et al.*, 2000]. More details of the WRF-chem/MOSAIC are described by *Fast et al.* [2006] and *Zaveri et al.* [2008]. More details of the ATRAS module are described by *Matsui et al.* [2011, 2013a, 2013b, 2014a, 2014b].

In this study, optical and radiative variables are calculated off-line. Aerosol extinction, single scattering albedo, and asymmetry factor are calculated for wavelengths of 300, 400, 600, and 999 nm (similar to the WRF-chem model) using the codes of *Bohren and Huffman* [1998] by assuming the shell-core representation (BHCOAT) for internally mixed BC particles and the well-mixed representation (BHMIE) for pure BC and BC-free particles. The enhancement of BC absorption is calculated in the BHCOAT. Using the optical calculations, shortwave radiative transfer is calculated for clear-sky conditions with the Goddard scheme (two-stream adding method based on *Chou* [1992]), which is used in the WRF-chem model.

Figure 2 shows the BC absorption enhancement ratio and critical supersaturation for each aerosol bin used in the ATRAS module. The values are calculated at the center of each aerosol bin (aerosol diameter and BC mass fraction) with the assumption that the coating is ammonium sulfate (dry conditions). The BC absorption enhancement ratio is calculated by using the BHCOAT and BHMIE codes, and the critical supersaturation is calculated by using the k-Köhler theory [*Petters and Kreidenweis*, 2007]. The BC absorption enhancement ratio is defined as the enhancement (increment) of BC absorption by coating species normalized by the absorption of the BC core only. The enhancement ratio increases with aerosol diameter and the mass fraction of coatings (Figure 2a, bottom right). The critical supersaturation (Figure 2b) is an indicator of CCN activity, and smaller (larger) critical supersaturation means more (less) CCN active. The fact that the critical supersaturation decreases with aerosol diameter and the mass fraction of coatings (Figure 2b) shows that BC-containing particles with larger diameters and larger amounts of coating have higher CCN activity. An important conclusion from Figure 2 is that absorption enhancement and CCN activity (which are important for estimating direct

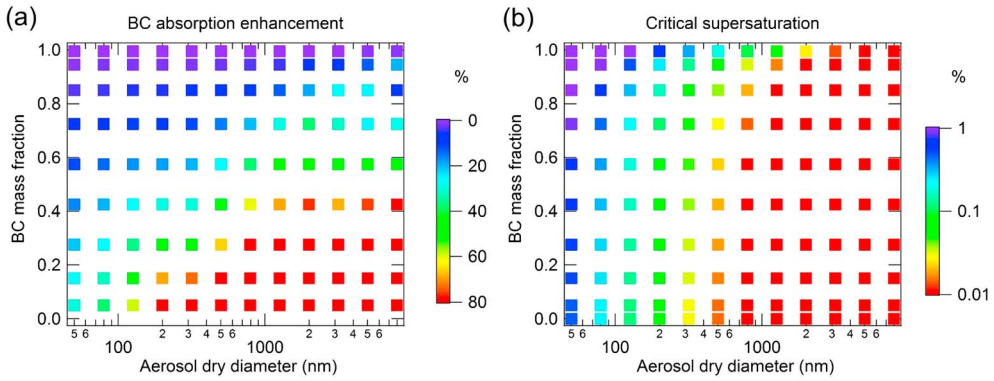

Figure 2. (a) BC absorption enhancement ratio and (b) critical supersaturation calculated for each aerosol bin in the ATRAS module. The values are calculated at the center of each aerosol bin (aerosol dry diameter and BC mass fraction) with the assumption that the coating is ammonium sulfate. BC absorption enhancement ratio is calculated for dry condition at the wavelength of 550 nm with the values of refractive index of 1.82 + 0.74i for BC and 1.50 + 0.0i for ammonium sulfate. Critical supersaturation is calculated with the κ values of 1×10^{-6} for BC and 0.5 for ammonium sulfate. Note that the values are calculated theoretically; they are not obtained from three-dimensional simulations.

and indirect effects, respectively) depend on both aerosol size and BC mixing state. This dependence can be resolved by use of a model with a two-dimensional bin representation such as ATRAS, which leads to more accurate calculation of absorption enhancement and CCN activity of BC-containing particles.

3. Simulation Setups

3.1. Domain and Period

The simulation domains and periods used in this study are the same as those used in previous studies [*Matsui et al.*, 2013a, 2013b, 2014a, 2014b]. Figure 3 shows the simulation domains. The horizontal grid spacing is 360 km for the outer domain (30 × 20 grids) and 120 km for the inner domain (39 × 24 grids), with 13 vertical layers from the surface to 100 hPa. A coarse grid resolution is used because the ATRAS module is computationally expensive [*Matsui et al.*, 2013a, 2014a]. The simulation period is from 21 March to 26 April 2009, and statistics are calculated for the model results from 24 March to 26 April. The National Centers for Environmental Prediction Final operational analysis data are used for initial and boundary conditions and for nudging (free troposphere only) of meteorological fields. The meteorological schemes used in this study are the rapid radiative transfer model longwave radiation scheme, the Goddard shortwave radiation scheme, the Monin-Obukhov surface layer scheme, the Noah land surface scheme, the Yonsei University planetary boundary layer scheme, the Kain-Fritsch cumulus cloud scheme, and the Morrison two-moment cloud microphysical scheme. The results of the inner domain are used to calculate statistics in this study. This study focuses on BC direct effect and does not evaluate BC indirect effect because the model does not consider cloud-aerosol interactions for convection (subgrid-scale wet removal) and the simulations are made with a coarse grid spacing.

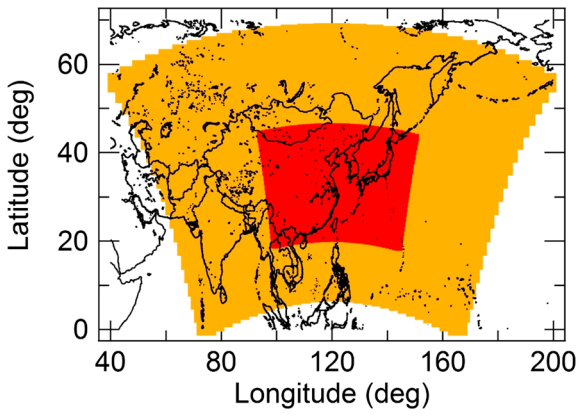

Figure 3. Simulation domains used in this study. The outer (orange) and inner (red) domains have horizontal grid spacings of 360 and 120 km, respectively.

3.2. Model Validation

The Aerosol Radiative Forcing in East Asia (A-FORCE) aircraft campaign was conducted over the Yellow Sea and the East China Sea during the simulation period [*Oshima et al.*, 2012; *Moteki et al.*, 2012]. Surface measurements were also conducted over the outflow region in Japan (at Fukue (32.75°N, 128.68°E) and Hedo (26.87°N, 128.25°E)) [*Takami et al.*, 2005,

Table 1. List of Simulations and Parameters for Emissions Used in This Study[a]

Simulation	Median Diameter (nm)		Sigma	Fext (%)[b]	SCinit[c]		Comments
	FF[d]	BF and BB[d]			FF	BF and BB	
Base	70	150	1.8	50	1.1	1.4	---
Size 1	30	50	1.8	50	1.1	1.4	Smaller diameter
Size 2	80	200	1.8	50	1.1	1.4	Larger diameter
Size 3	70	150	1.6	50	1.1	1.4	Smaller sigma
Size 4	70	150	2.0	50	1.1	1.4	Larger sigma
Size 5	30	50	1.6	50	1.1	1.4	Smaller diameter, smaller sigma
Size 6	30	50	2.0	50	1.1	1.4	Smaller diameter, larger sigma
Size 7	80	200	1.6	50	1.1	1.4	Larger diameter, smaller sigma
Size 8	80	200	2.0	50	1.1	1.4	Larger diameter, larger sigma
Mixing State 1	70	150	1.8	100	---	---	Externally mixed BC
Mixing State 2	70	150	1.8	0	1.1	1.4	Internally mixed BC
Mixing State 3	70	150	1.8	50	1.05	1.2	Less coating
Mixing State 4	70	150	1.8	50	1.2	1.6	More coating
Mixing State 5	70	150	1.8	0	1.05	1.2	Internally mixed BC, less coating
Mixing State 6	70	150	1.8	0	1.2	1.6	Internally mixed BC, more coating

[a]Both coagulation-on and coagulation-off simulations are conducted for each simulation.
[b]Fext is the fraction of externally mixed BC in emissions.
[c]SCinit is the shell-core diameter ratio in emissions. A higher (lower) SC ratio means BC particles with larger (smaller) amounts of coating by non-BC species.
[d]FF, BF, and BB denote fossil fuel, biofuel, and biomass burning, respectively.

2007; *Kondo et al.*, 2011a]. Model simulations during this period have been validated by using these measurements [*Matsui et al.*, 2013a, 2013b, 2014a, 2014b]. Model simulations reproduced BC and sulfate mass concentrations and their temporal variations at the Fukue and Hedo sites reasonably well. Model simulations also reproduced the vertical profiles of the mass and number concentrations of BC particles and the volume and number concentrations of light scattering particles (BC-free particles) during the A-FORCE campaign. The ATRAS module simulated detailed information about the BC mixing state for the first time, and it successfully captured the observed BC mixing state, including the size-dependent number fractions of BC-containing and BC-free particles and the coating thickness of BC-containing particles [*Matsui et al.*, 2013a, 2014a]. A better simulation of aerosol number concentrations ($>$10 nm) was obtained by resolving new particle formation processes [*Matsui et al.*, 2013b, 2014a]. The model performance of organic aerosol simulations was also much improved at Fukue and Hedo by use of the volatility-basis set approach [*Matsui et al.*, 2014b]. A validation of aerosol optical parameters is being conducted as part of another study (M. Koike et al., in preparation, 2016), and in that study the model has simulated realistic values of single scattering albedo and aerosol optical thickness over East Asia (not shown). Based on these previous model evaluations, this study does not present any further about model validations.

3.3. Emissions

The emission inventories used in this study are also similar to the inventories used in previous studies [*Matsui et al.*, 2014a]. The anthropogenic and volcanic emissions are taken from *Streets et al.* [2003], with a modification for the emissions from the Miyakejima volcano [*Matsui et al.*, 2013b]. These emissions are assumed to be constant during the simulation period. Daily biomass burning emissions are taken from the Global Fire Emissions Database version 3 [*van der Werf et al.*, 2010]. Biogenic emissions are calculated online using the Model of Emissions of Gases and Aerosols from Nature version 2 [*Guenther et al.*, 2006]. This study, like previous studies [*Matsui et al.*, 2013a, 2014a], does not consider online dust and sea salt emissions from natural sources. A sensitivity simulation showed that the change in BC direct radiative effect due to consideration of these dust and sea salt emissions was small enough (less than 10%) over the East Asian region during the simulation period.

Based on previous measurements and modeling studies [*Kondo et al.*, 2011b, 2011c; *Matsui et al.*, 2011; *Reddington et al.*, 2011], primary emissions in the base simulation are assumed to have a number (count) median diameter (CMD) of 70 nm for fossil fuel (FF) sources and a CMD of 150 nm for biofuel (BF) and biomass burning (BB) sources, with a standard deviation (sigma) of 1.8 (Table 1). The simulation with these parameters generally reproduced the BC number size distribution during the A-FORCE aircraft campaign; the mean values of simulated CMD (100 nm) and sigma (1.5) along the flight tracks are within the range of observed CMD (100–130 nm) and sigma (1.5–1.6) [*Moteki et al.*, 2012]. Because FF and BF sources are not separated in the anthropogenic emissions used in this study, the fractions of FF and BF in the anthropogenic emissions are derived from the global data set

of *Bond et al.* [2007] for BC and organic aerosols. BC emissions are given as both externally mixed BC (pure BC) and internally mixed BC (BC + organic aerosols), and pure BC is assumed to be 50% of total BC (for all sources) based on a measurement near emission sources [*Matsui et al.*, 2013a]. For internally mixed BC particles, the shell (all species under dry conditions) to core (BC) diameter ratio is assumed to be 1.1 for FF sources and 1.4 for BB and BF sources based on *Kondo et al.* [2011b, 2011c]. Though the shell-to-core diameter ratio for internally mixed BC particles in emissions should be characterized by a frequency distribution rather than being constant [*Kondo et al.*, 2011b, 2011c; *Matsui et al.*, 2013a], this study assumes a constant ratio because information about the frequency distribution of the ratio is limited.

In this study, all aerosol emissions are given as particles from 40 nm to 10 μm in dry diameter. There are no primary particles less than 40 nm in diameter. The mass flux of particles less than 40 nm in the lognormal size distribution for emissions is given to the smallest two-dimensional bins (bins for particles at 40–63 nm in diameter). The main conclusions obtained in this study are not changed by the treatment of emitted particles less than 40 nm in diameter.

3.4. Sensitivity Simulations

To evaluate the impact of uncertainties in the size distribution and mixing state in emissions on BC and its optical and radiative variables (section 4.2), 14 sensitivity simulations are conducted with different emission parameters (Table 1). In these sensitivity simulations, the mass flux of BC emissions is the same as that of the base simulation. To evaluate the effect of variations in the size distribution of primary emissions, eight sensitivity simulations are conducted (Size 1–8 in Table 1); the CMD values ranged between 30 and 80 nm for FF sources and between 50 and 200 nm for BF and BB sources, and the sigma values ranged between 1.6 and 2.0. These ranges of values are determined from ranges of uncertainty in previous studies [*Reddington et al.*, 2011; *Carslaw et al.*, 2013]. The minimum CMD value of 30 nm (for FF sources) is used in this study, though it is small for primary emission of BC particles in a large-scale model [*Reddington et al.*, 2013]. To investigate the impact of variations of the BC mixing state in emissions, six sensitivity simulations are conducted (Mixing State 1–6 in Table 1); the percentages of pure BC ranged between 0% and 100%, and the shell-core diameter ratios of internally mixed BC particles ranged between 1.05 and 1.2 for FF sources and between 1.2 and 1.6 for BF and BB sources. The ranges of these values are taken from the limited measurements of BC mixing states by *Kondo et al.* [2011b, 2011c].

The importance of coagulation processes is discussed in section 4.3. Sensitivity simulations without coagulation processes (coagulation-off) are also conducted for each of 15 combinations of parameters listed in Table 1 (including the base case simulation).

3.5. Definition of Variables

This study uses BC mass concentrations in column (column BC), mass concentrations of particulate matter smaller than 2.5 μm in diameter ($PM_{2.5}$), CCN concentrations at supersaturations of 1.0% ($CCN_{1.0}$) and 0.1% ($CCN_{0.1}$), aerosol optical depth (AOD), absorption aerosol optical depth (AAOD), the enhancement ratio of BC absorption by coatings (Eabs), mass absorption cross section (MAC), and BC direct radiative effect at the surface (DRE_{surf}), at the top of the atmosphere (DRE_{toa}), and in the atmosphere (DRE_{atmos}). The values of aerosol optical properties (AOD, AAOD, Eabs, and MAC) are shown at a wavelength of 600 nm. The MAC is the ratio of AAOD to column BC. Eabs is the enhancement (increment) of AAOD by coating species normalized by AAOD without a coating (BC only, or externally mixed BC). The domain- and period-averaged values of Eabs and MAC are calculated from the ratio between the average of the numerator (AAOD) and the average of the denominator (AAOD of externally mixed BC or column BC). The BC direct radiative effect is calculated from the difference of the radiative flux between the calculations with the imaginary part of the BC refractive index of 0.74 and 0. The BC direct radiative effect therefore does not include the changes in flux by BC scattering. The BC direct radiative effect is calculated off-line with two mixing state treatments: one is the mixing-state-resolved calculation using the information in the model simulations (with the absorption enhancement) and the other is the calculation without the coating species (externally mixed treatment without the absorption enhancement). In the externally mixed calculations, one internally mixed particle is separated into two smaller particles, a pure BC particle and a BC-free particle. Total mass concentrations of each species are conserved, but number concentrations of internally mixed particles are doubled in the calculations [*Matsui et al.*, 2013a, 2014a]. The results obtained from the externally mixed treatment are used in section 4.4.

In sections 4.2 and 4.3, the "variability" of variables is used to assess uncertainties in the treatment of emissions. The variability is calculated for each variable (e.g., column BC, AAOD) as a domain- and period-averaged value. The maximum and minimum values of the variability are defined as

$$V_{p,\max} = \frac{\max(p_{sens}) - p_{base}}{p_{base}}, V_{p,\min} = \frac{\min(p_{sens}) - p_{base}}{p_{base}}. \quad (1)$$

where $V_{P,\max}$ ($V_{P,\min}$) is the maximum (minimum) value of the variability range for variable P and P_{base} (P_{sens}) is the domain- and period-averaged absolute value (>0) of variable P in the base (sensitivity) simulations. These simple definitions are used in this study, though the uncertainty may be larger when considering interactions between the parameters [*Lee et al.*, 2012, 2013]. The variability is calculated separately for the size distributions (eight simulations, Size 1–8 in Table 1) and for the mixing states (six simulations, Mixing State 1–6 in Table 1). In sections 4.3 and 4.4, the total variability is also defined and used. The total variability is simply defined as the sum of the variability for the size distribution and for the mixing state, by assuming that the two variabilities are independent of each other. The variability is also calculated for the sensitivity simulations without coagulation processes in section 4.3. In that calculation, the base simulation without coagulation is used for the normalization (not the base simulation with coagulation).

4. Simulation Results

4.1. Base Case Simulation

Figure 4 shows the period-averaged distributions of BC mass concentrations and optical/radiative variables in the base case simulation. All hourly model outputs from 00:00 to 23:00 universal time (UT) are used in the calculations for this figure and statistics ("Mean value" in Table 2). The distribution of column BC and AAOD reflects the distribution of BC emission inventories (Figures 4a and 4b). Both column BC and AAOD reach maxima over China and decrease with transport to the outflow region. The period- and domain-averaged column BC and AAOD values are 1405 $\mu g\,m^{-2}$ and 0.013, respectively (Table 2).

Eabs and MAC are lower near the emission sources (over the Asian continent) and increase gradually with transport to the outflow region (over the Yellow Sea, the East China Sea, and the western Pacific) (Figures 4c and 4d). This result reflects BC absorption enhancement by both condensation and coagulation processes during transport. Aged BC particles, which have higher absorption efficiency and higher CCN activity, are easier to activate and remove from the atmosphere than fresh BC particles (Figure 2). Figures 4c and 4d show the net effect of absorption enhancement (which increases Eabs and MAC) and wet removal of aged BC particles (which decreases Eabs and MAC). The values of Eabs are 50–65% near the emission sources and 70–80% over the outflow region (Figure 4c). The values of MAC are 8.5–9.5 $m^2\,g^{-1}$ near the emission sources and 9.5–10.5 $m^2\,g^{-1}$ over the outflow region (Figure 4d). The period- and domain-averaged Eabs and MAC values are 65.3% and 9.4 $m^2\,g^{-1}$, respectively (Table 2). These values are within the ranges reported in previous studies [*Bond et al.*, 2013].

The distribution of BC direct radiative effect is generally similar to that of the BC mass concentrations (Figures 4e and 4f). The period- and domain-averaged DRE_{surf} and DRE_{toa} values are $-3.6\,W\,m^{-2}$ and $2.2\,W\,m^{-2}$, respectively, with the minimum/maximum values of $-8\,W\,m^{-2}$ and $8\,W\,m^{-2}$ over China. The DRE_{toa} value ($2.2\,W\,m^{-2}$) is larger than the global average BC direct radiative effect (e.g., $0.88\,W\,m^{-2}$ in *Bond et al.* [2013]) though the definition and the method to estimate BC direct radiative effect used in this study are not exactly the same as those used in previous studies. The results show the importance of BC climate impacts on a regional scale over East Asia.

4.2. Variability of BC Variables

Figure 5 shows the ranges of variability of BC mass concentrations and optical/radiative variables estimated from the eight sensitivity simulations for the size distribution and six sensitivity simulations for the mixing state. The variability is calculated by using the data at 03:00 UT (around noon) because the off-line optical calculations for all the simulations are computationally heavy.

The variability associated with size distribution is larger than that associated with mixing state for all the variables shown in Figure 5. The variability associated with size distribution is estimated to be 16% for

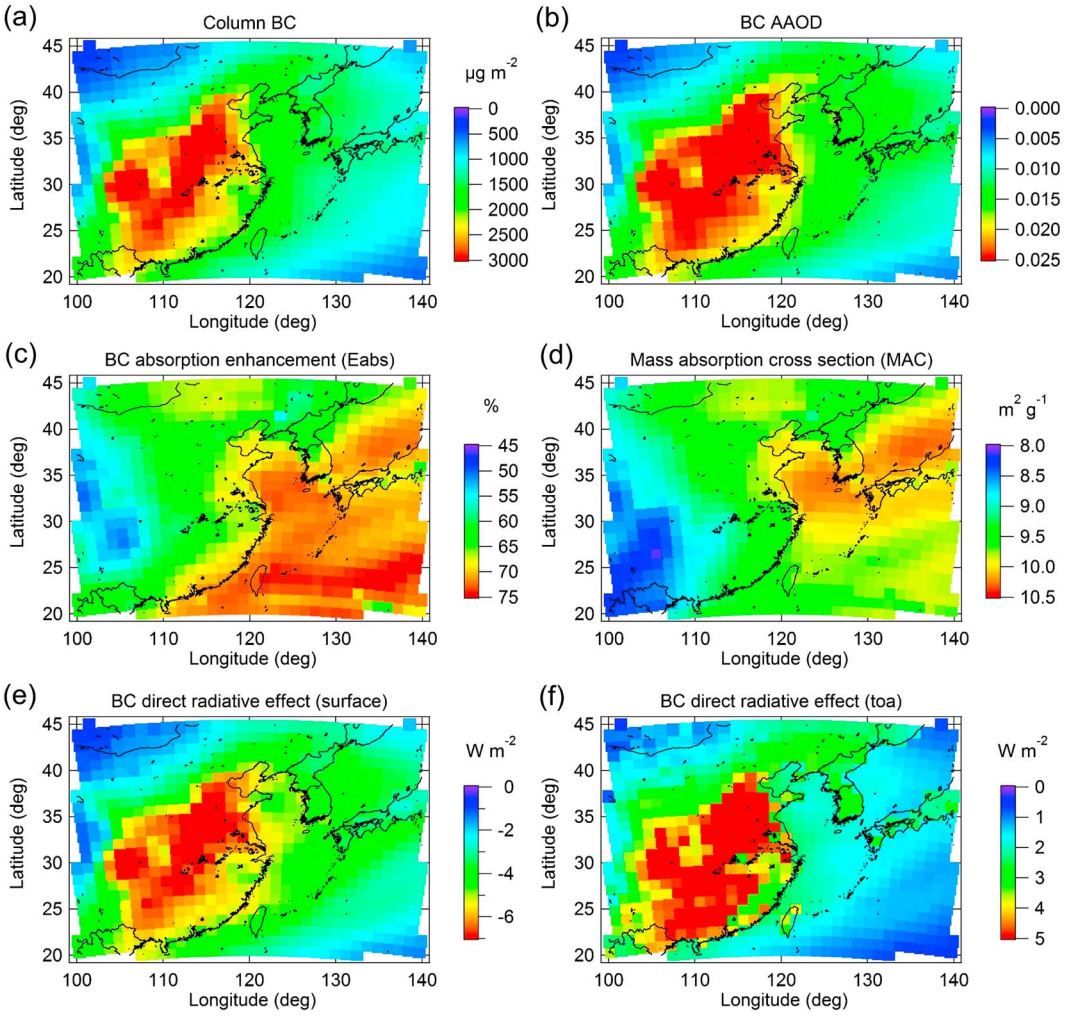

Figure 4. The period-averaged distributions of (a) column BC, (b) AAOD, (c) Eabs, (d) MAC, (e) DRE_{surf}, and (f) DRE_{toa}. Each variable is defined in section 3.5.

Table 2. Period- and Domain-Averaged Values of Aerosol Parameters and Their Variability

			Variability (%)			
Parameter[a]	Unit	Mean Value	Size	Mixing State	Total (Coagulation-On)	Total (Coagulation-Off)
$CCN_{0.1}$	cm^{-3}	396	16.4	0.94	17.4	95.8
$CCN_{1.0}$	cm^{-3}	2191	100.2	0.78	100.9	1400
$PM_{2.5}$	$\mu g\ m^{-3}$	12.3	4.5	0.21	4.7	12.8
BC	$\mu g\ m^{-2}$	1405	15.5	4.6	20.1	43.2
AOD	---	0.25	9.2	0.66	9.9	72.1
Eabs	%	65.3	56.5	42.0	98.5	98.5
AAOD	---	0.013	64.0	21.5	85.6	76.7
MAC	$m^2\ g^{-1}$	9.4	48.6	26.2	74.8	55.9
RF_{surf}	$W\ m^{-2}$	−3.6	64.8	21.9	86.7	80.3
RF_{toa}	$W\ m^{-2}$	2.2	41.9	16.1	58.0	54.2
RF_{atmos}	$W\ m^{-2}$	5.8	56.1	19.7	75.8	70.3

[a]The values at 1 km (sigma = 0.895) are shown for $CCN_{1.0}$, $CCN_{1.0}$, and $PM_{2.5}$. The values in column are shown for AOD, Eabs, AAOD, and MAC.

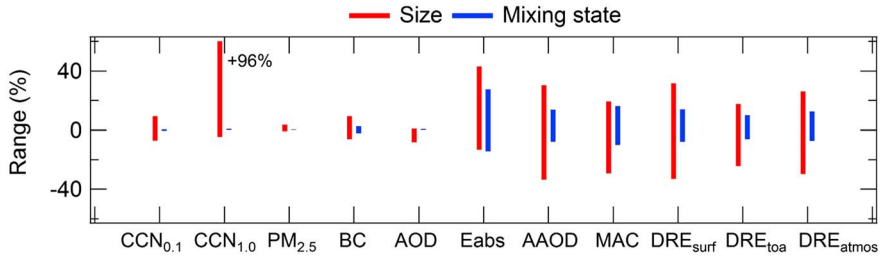

Figure 5. The ranges of variability of BC mass concentrations, optical properties, and direct radiative effects associated with particle size distributions (red, estimated from eight sensitivity simulations) and mixing states (blue, estimated from six sensitivity simulations) in emissions. Variability is defined in section 3.4.

the column BC, 49–64% for optical variables (E_{abs}, AAOD, and MAC), and 42–65% for BC direct radiative effect (DRE_{surf}, DRE_{toa}, and DRE_{atmos}). These results underscore the importance of accurately describing the size distribution of emissions in simulating BC mass concentrations and optical/radiative variables in a model, though the absolute values of the variability depend on the uncertainty ranges given in Table 1. The variability associated with mixing state is also important, especially for the Eabs value (42%, Table 2), which is generally equivalent to the variability associated with size distribution (57%, Table 2). The variability for Eabs associated with mixing state is the cause of the variability of other optical and radiative variables associated with the mixing state (16–26%, Table 2).

The total variability caused by uncertainties in the size distribution and mixing state parameters is larger in the BC optical (75–99%) and radiative (58–87%) variables than in the BC mass concentrations (20%) (Table 2 and Figure 6). This result shows the importance of accurate treatment of the size distribution and the mixing state in emissions in calculating BC optical and radiative variables in a model. In contrast, the variability of the BC mass concentration is much smaller (20%). Because BC mass concentrations are mainly controlled by emission, transport, and removal processes, it is very important to accurately calculate the change of CCN activity due to aging processes. In addition to these processes, the absorption of solar radiation (including its enhancement during transport) is also important for the calculation of optical and radiative variables. The threefold to fivefold greater sensitivity of the optical and radiative variables (than of BC mass concentrations) to the size distribution and mixing state parameters therefore suggests that a three-dimensional model should resolve BC absorption and its enhancement by aging processes for more accurate estimation of BC and its radiative effect, in addition to the treatment of CCN activity (hydrophobic-hydrophilic conversion) and wet removal. The cause of the different variability between BC mass concentrations and the optical/radiative variables is discussed in section 4.3.

4.3. The Cause of Different Variability Between BC Mass and Optical/Radiative Variables

Figure 6 shows the range of total variability of each variable for both the coagulation-on and coagulation-off simulations. The variables for mass and number concentrations (BC, $PM_{2.5}$, $CCN_{1.0}$, and $CCN_{0.1}$) and the variables for optical properties and radiative effects related to absorption (Eabs, AAOD, MAC, DRE_{surf}, DRE_{toa}, and DRE_{atmos}) have distinctly different characteristics. The total variability of the mass/number variables differs between the coagulation-on and the coagulation-off simulations. The variability is considerably smaller in the coagulation-on simulations. For instance, the variability of BC mass concentrations is 43% for the

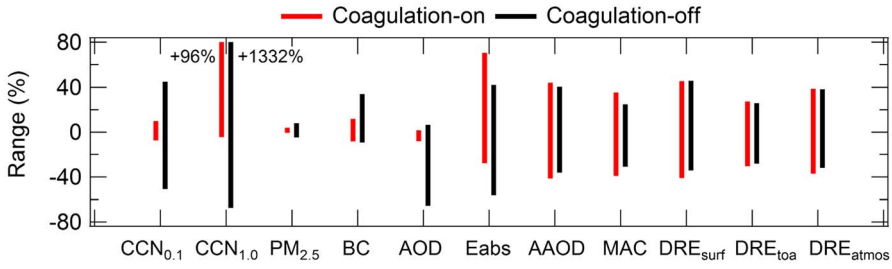

Figure 6. The total ranges of variability (the sum of the size and the mixing state variability) for each variable estimated from sensitivity simulations with (coagulation-on, red) and without (coagulation-off, black) coagulation processes.

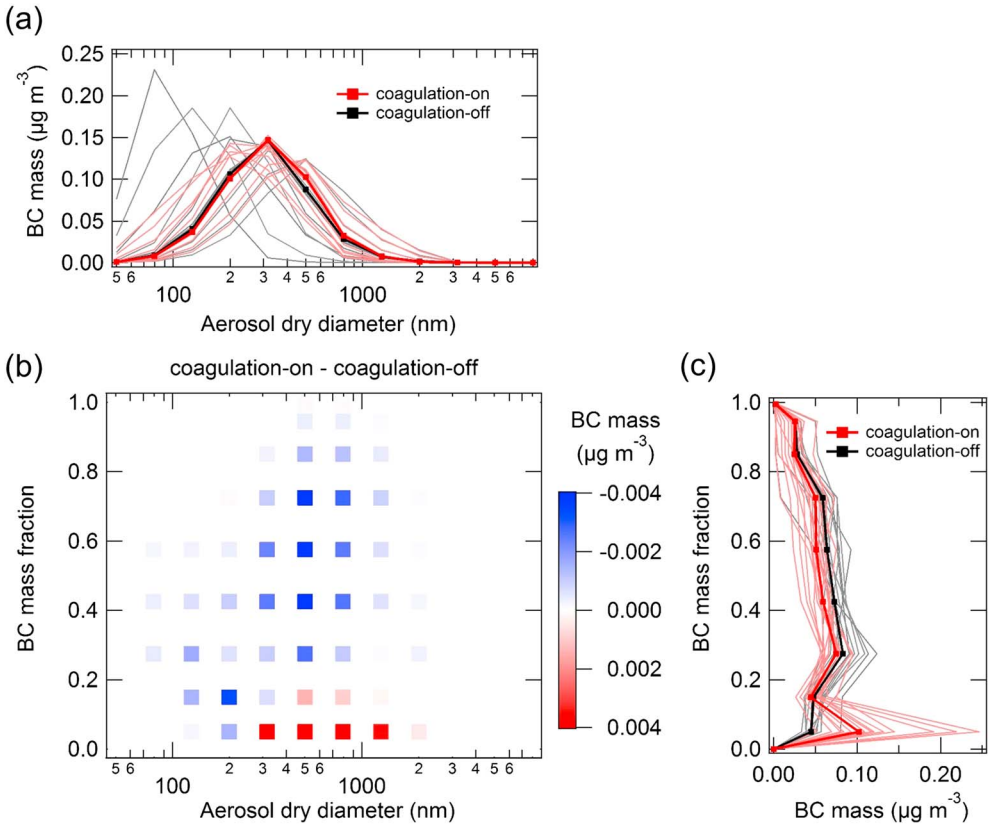

Figure 7. The period- and domain-averaged BC mass concentrations at a sigma level of 0.895 (~ 1 km): (a) the size distributions for all coagulation-on (red) and coagulation-off (black) simulations, which are calculated from BC mass summed over all mixing state bins (for each size bin), (b) the difference in BC mass due to coagulation (between the base simulations with and without coagulation) for each size and mixing state bin in the ATRAS module, and (c) the mixing state distribution for all coagulation-on (red) and coagulation-off (black) simulations, which are calculated from BC mass summed over all size bins (for each mixing state bin). The thick black and red lines in Figures 7a and 7c show the results of the base simulation.

coagulation-off simulations but only 20% for the coagulation-on simulations (Table 2 and Figure 6). In contrast, the variability of the optical/radiative variables is similar in the coagulation-on (58–99%) and the coagulation-off simulations (54–99%). These results suggest that coagulation is one of the important causes of the difference in variability between the mass/number variables and the optical/radiative variables.

To elucidate the cause of this difference, the impact of coagulation on aerosol size distribution and BC mixing state is examined. Figure 7b shows the change in BC mass concentrations due to coagulation within the two-dimensional bin field in the ATRAS module (domain and period average). Coagulation decreases BC particles that have a relatively small size and large BC mass fraction (less aged BC) and increases BC particles that have a relatively large size and small BC mass fraction (more aged BC). This result is consistent with previous box modeling studies [*Riemer et al.*, 2010; *Zaveri et al.*, 2010].

Figure 7a shows the size distributions of BC mass concentrations for all coagulation-on and coagulation-off simulations (domain and period average). These size distributions are calculated from BC mass summed over all mixing state bins. These distributions are useful for interpreting the variability of BC mass concentrations because the CCN activity of BC-containing particles is more sensitive to the size than to the mixing state (Figure 2b). Coagulation is especially important (the difference between coagulation-on and coagulation-off simulations is large) when the values of the CMDs of emissions are small. This result is consistent with box-modeling results [*Fierce et al.*, 2013]. The BC mass size distributions are highly variable in the coagulation-off simulations (especially for particles less than 200 nm in diameter) because of the large difference in the size distributions in emissions. In contrast, the BC mass size distributions are less variable in the coagulation-on simulations. The BC mass size distributions therefore become less scattered due to

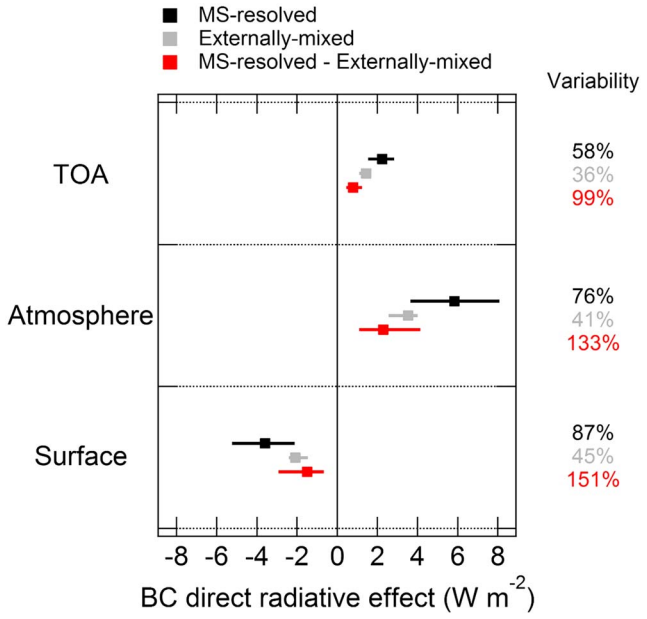

Figure 8. The period- and domain-averaged BC direct radiative effects by absorption (squares) at the top of the atmosphere, in the atmosphere, and at the surface. BC direct radiative effect is shown for the off-line optical and radiative calculations with the coating species (mixing state resolved, black) and without the coating species (BC only, gray). The differences between the two calculations are also shown (red). The horizontal bars show the ranges of uncertainty (variability) estimated from 14 sensitivity simulations.

coagulation growth, and it reduces the variability of CCN activity and removal rate of BC. As a result, the BC mass concentrations are less sensitive to emissions in the simulations with coagulation.

Figure 7c shows BC mass concentrations as a function of BC mixing state (BC mass fraction) for all coagulation-on and coagulation-off simulations. These mixing state distributions are calculated from BC mass summed over size bins. These distributions are useful for interpreting the variability of BC optical properties because the absorption enhancement is more sensitive to the mixing state (Figure 2a) than the CCN activity of BC-containing particles (Figure 2b). The mass concentrations of aged BC particles (small BC mass fractions) are less variable in the coagulation-off simulations, whereas they are much more scattered in the coagulation-on simulations. This result shows that the formation rate of aged BC particles by coagulation is largely dependent on the size and the mixing state in emissions. Because these particles have higher absorption efficiencies, the variability of aged BC mass associated with coagulation is one of the causes of the larger variability of BC optical and radiative variables. The similar variability of the optical properties (Eabs, AAOD, and MAC) between the coagulation-on and coagulation-off simulations (Figure 6) can be explained by the cancellation of the two coagulation effects: one is the reduction of the variability of the BC mass size distribution (Figure 7a) and the other is the enhancement of the variability of the aged BC mass (Figure 7c).

As shown above, the impact of coagulation on the variability is completely different for BC mass concentrations and optical/radiative variables. The cause of this difference is the contrasting impact of coagulation on aerosol size and BC mixing state. This study evaluates the complicated responses of aerosol microphysical processes for the first time by using an aerosol model that can resolve both aerosol size distributions and BC mixing states and that can explicitly calculate aging processes such as condensation and coagulation and the resulting enhancement of absorption and CCN activity.

In this study, the optical and radiative variables are calculated by assuming the shell-core particle type for all internally mixed BC particles. In the real atmosphere, coagulation could make noncoated BC particles by attachment of BC to non-BC species (attached BC particles). Such particles have less absorption efficiency than the particles with the shell-core assumption [*Fuller et al.*, 1999]. If the contribution of the attached BC particles is not negligible, the shell-core assumption overestimates BC absorption. However, the A-FORCE observations show that the fraction of attached BC particles was less than 5% over the outflow region in East Asia (N. Moteki, personal communication, 2015). This result suggests that the shell-core assumption used in this study is reasonable, at least over the outflow region in East Asia during the simulation periods.

4.4. Radiative Effect and Its Uncertainty

Figure 8 shows the period- and domain-averaged BC direct radiative effect (DRE_{toa}, DRE_{atmos}, and DRE_{surf}) and its variability (uncertainty). The mean value is calculated from the base case simulation (using the data from 00:00 to 23:00 UT, as shown in section 4.1), and the variability (uncertainty) is calculated from the variability of the sensitivity simulations (using the data at 03:00 UT, as shown in section 4.2). The ranges of

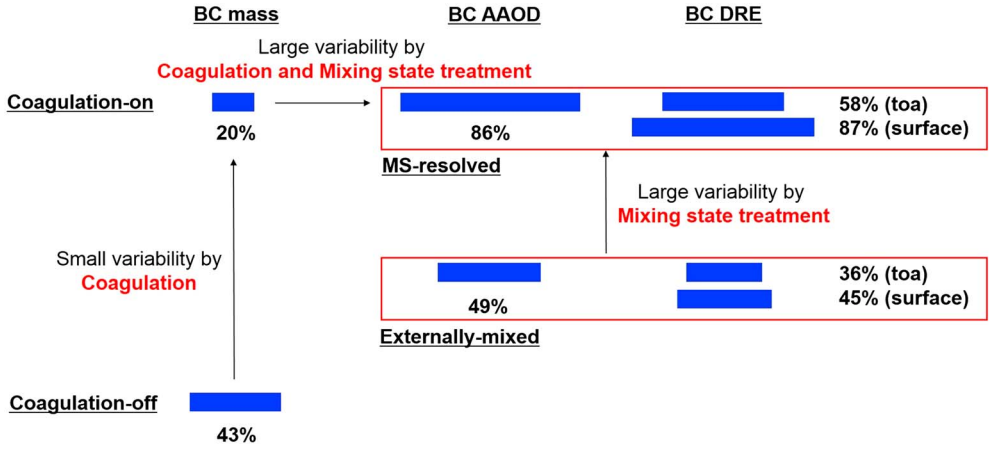

Figure 9. Summary of the variability values (shown by blue bars) estimated in this study with information about important processes and treatments for the variability.

uncertainty of DRE_{toa}, DRE_{atmos}, and DRE_{surf} are 1.5–2.8 W m^{-2}, 3.7–8.1 W m^{-2}, and from −5.2 to −2.1 W m^{-2}, respectively. The high sensitivity of BC direct radiative effect to the size and the mixing state in emissions shows their importance in the evaluation of BC radiative effect.

The uncertainties of BC direct radiative effect differed between the optical calculations with (mixing state resolved) and without (externally mixed BC, BC core only) absorption enhancement. The mixing-state-resolved calculations increase both the absolute values and the uncertainties of BC direct radiative effect compared with the externally mixed calculations (Figure 8); the uncertainties increase from 36% to 58% at the top of the atmosphere, from 41% to 76% in the atmosphere, and from 45% to 87% at the surface. In addition, the increments by resolving BC mixing state (the difference between the two calculations, shown by red in Figure 8) have the highest sensitivity to the size and mixing state in emissions (the variability of the increments was calculated from the increments of 15 model simulations using the definition in section 3.5). These results show the importance of resolving the enhancement of BC absorption sufficiently in a model based on aerosol microphysical and chemical processes and the importance of reducing the uncertainties in the size and the mixing state in emissions for more accurate estimation of BC radiative effect.

Figure 9 summarizes the results and findings of this study. The optical/radiative variables are highly sensitive to the size and the mixing state in emissions (the variability is 58–99%). This sensitivity of the optical/radiative variables was 3 to 5 times that of the mass/number variables (section 4.2). This study identified the importance of two effects that were responsible for this difference: (1) reduction of the variability of BC mass concentrations (the mass/number variables) due to coagulation (section 4.3) and (2) enhancement of the variability of BC direct radiative effect (the optical/radiative variables) by resolving BC mixing state (section 4.4).

5. Summary and Conclusions

This study evaluated the uncertainties in the simulations of BC and its radiative effects by using the size- and the mixing-state-resolved three-dimensional model, WRF-chem/ATRAS-MOSAIC. This model can calculate a series of BC processes in the atmosphere, such as aging and removal processes of BC-containing particles, with the enhancement of absorption and CCN activity based on aerosol microphysical and chemical processes. The simulations were conducted over East Asia and its outflow region in spring 2009, when the simulated mass concentrations, number concentrations, and mixing states of aerosols had already been validated by aircraft and surface measurements. The period- and domain-averaged column BC, AAOD, Eabs, and MAC were 1405 μg m^{-2}, 0.013, 65%, and 9.4 m^2 g^{-1}, respectively, in the base case simulation. The BC direct radiative effect by absorption was 2.2 W m^{-2} at the top of the atmosphere, 5.8 W m^{-2} in the atmosphere, and −3.6 W m^{-2} at the surface.

The uncertainties in BC and its radiative effects were estimated from 14 sensitivity simulations that considered the uncertainties in the particle size (the median diameter and the sigma of the size distribution) and the mixing state (the fraction of pure BC and internally mixed BC particles and the shell-core diameter ratio of internally mixed BC) in emissions. The uncertainties were defined on the basis of previous studies. The optical and

radiative variables (Eabs, AAOD, MAC, and BC direct radiative effect) were highly sensitive to the aerosol size and mixing state in emissions, and the variability of these variables was estimated to be 58–99% (period and domain average). The fact that this range of variability corresponded to BC direct radiative effect over East Asia and its outflow region of 1.5–2.8 W m^{-2} at the top of the atmosphere, 3.7–8.1 W m^{-2} in the atmosphere, and from −5.2 to −2.1 W m^{-2} at the surface (period and domain average) showed the importance of the treatment of the initial aerosol size and the mixing state in estimating BC radiative effect accurately. Because the uncertainty of BC direct radiative effect is large, a more complex response to the size and mixing state in emissions may be expected when aerosol-radiation interactions are calculated online.

In contrast, the variability of BC mass concentrations was only 20%, much smaller than that of BC optical and radiative variables. Therefore, the optical and radiative variables were more sensitive than BC mass concentrations to the aerosol size and the mixing state in emissions. The main causes of the difference in sensitivity (variability) of the BC mass concentrations and the optical/radiative variables were (1) reduction of the variability of the BC mass concentrations by coagulation and (2) enhancement of the variability of BC absorption by resolving BC mixing state. These complicated responses of aerosol microphysical processes were calculated and evaluated for the first time by use of a detailed three-dimensional aerosol model. The results shown in this study suggest that the following two points are important in the estimation of BC radiative effect: (1) reduction of the uncertainties in the aerosol size distribution and the mixing state in emissions and (2) improvement of the representation of BC mixing state and absorption enhancement in aerosol models because most models do not treat them sufficiently.

Acknowledgments

H. Matsui was supported by the Japan Society for the Promotion of Science (JSPS) Postdoctoral Fellowships for Research Abroad. This work was supported by the Ministry of Education, Culture, Sports, Science, and Technology and the Japan Society for the Promotion of Science (MEXT/JSPS) KAKENHI grants 26740014 and 26241003 and MEXT Green Network of Excellence (GRENE) and Arctic Challenge for Sustainability (ArCS) projects. This work was also supported by the environment research and technology development fund of the Ministry of the Environment, Japan (2-1403). The author thanks Nobuhiro Moteki (University of Tokyo) for providing the useful comments on the attached BC particles and their optical properties observed during the A-FORCE campaign. The model simulations were conducted using the MSTSC super computer system at the Japan Agency for Marine-Earth Science and Technology. Data can be obtained by contacting H. Matsui (matsui@nagoya-u.jp). The author would like to thank the three anonymous reviewers of this manuscript for their useful and helpful suggestions.

References

Abdul-Razzak, H., and S. J. Ghan (2000), A parameterization of aerosol activation: 2. Multiple aerosol types, *J. Geophys. Res.*, *105*(D5), 6837–6844, doi:10.1029/1999JD901161.

Bohren, C. F., and D. R. Huffman (1998), *Absorption and Scattering of Light by Small Particles*, 530 pp., John Wiley, Hoboken, N. J.

Bond, T. C., D. G. Streets, K. F. Yarber, S. M. Nelson, J. H. Woo, and Z. Klimont (2004), A technology-based global inventory of black and organic carbon emissions from combustion, *J. Geophys. Res.*, *109*, D14203, doi:10.1029/2003JD003697.

Bond, T. C., G. Habib, and R. W. Bergstrom (2006), Limitations in the enhancement of visible light absorption due to mixing state, *J. Geophys. Res.*, *111*, D20211, doi:10.1029/2006JD007315.

Bond, T. C., E. Bhardwaj, R. Dong, R. Jogani, S. K. Jung, C. Roden, D. G. Streets, and N. M. Trautmann (2007), Historical emissions of black and organic carbon aerosol from energy-related combustion, 1850–2000, *Global Biogeochem. Cycles*, *21*, GB2018, doi:10.1029/2006GB002840.

Bond, T. C., et al. (2013), Bounding the role of black carbon in the climate system: A scientific assessment, *J. Geophys. Res. Atmos.*, *118*, 5380–5552, doi:10.1002/jgrd.50171.

Boucher, O., et al. (2013), Clouds and aerosols, in *Climate Change 2013: The Physical Science Basis. Contribution of Working Group I to the Fifth Assessment Report of the Intergovernmental Panel on Climate Change*, edited by T. F. Stocker et al., Cambridge Univ. Press, Cambridge, U. K., and New York.

Carslaw, K. S., et al. (2013), Large contribution of natural aerosols to uncertainty in indirect forcing, *Nature*, *503*, 67–71.

Carter, W. P. L. (2000), Documentation of the SAPRC-99 chemical mechanism for VOC reactivity assessment, Report to the California Air Resources Board. College of Engineering, Center for Environ. Res. and Tech., Univ. of California at Riverside, Calif. Contracts 92–329 and 95–308. [Available at: http://www.cert.ucr.edu/~carter/reactdat.htm.]

Chou, M. D. (1992), A solar radiation model for use in climate studies, *J. Atmos. Sci.*, *49*, 762–772.

Easter, R. C., S. J. Ghan, Y. Zhang, R. D. Saylor, E. G. Chapman, N. S. Laulainen, H. Abdul-Razzak, L. R. Leung, X. Bian, and R. A. Zaveri (2004), MIRAGE: Model description and evaluation of aerosols and trace gases, *J. Geophys. Res.*, *109*, D20210, doi:10.1029/2004JD004571.

Fahey, K. M., and S. N. Pandis (2001), Optimizing model performance: Variable size resolution in cloud chemistry modeling, *Atmos. Environ.*, *35*, 4471–4478.

Fast, J. D., W. I. Gustafson Jr., R. C. Easter, R. A. Zaveri, J. C. Barnard, E. G. Chapman, G. A. Grell, and S. E. Peckham (2006), Evolution of ozone, particulates, and aerosol direct radiative forcing in the vicinity of Houston using a fully coupled meteorology-chemistry-aerosol model, *J. Geophys. Res.*, *111*, D21305, doi:10.1029/2005JD006721.

Fierce, L., N. Riemer, and T. C. Bond (2013), When is cloud condensation nuclei activity sensitive to particle characteristics at emission?, *J. Geophys. Res. Atmos.*, *118*, 13,476–13,488, doi:10.1002/2013JD020608.

Fuller, K. A., W. C. Malm, and S. M. Kreidenweis (1999), Effects of mixing on extinction by carbonaceous particles, *J. Geophys. Res.*, *104*(D13), 15,941–15,954, doi:10.1029/1998JD100069.

Grell, G. A., S. E. Peckham, R. Schmitz, S. A. McKeen, G. Frost, W. C. Skamarock, and B. Eder (2005), Fully coupled "online" chemistry within the WRF model, *Atmos. Environ.*, *39*, 6957–6975.

Guenther, A., T. Karl, P. Harley, C. Wiedinmyer, P. I. Palmer, and C. Geron (2006), Estimates of global terrestrial isoprene emissions using MEGAN (Model of Emissions of Gases and Aerosols from Nature), *Atmos. Chem. Phys.*, *6*, 3181–3210.

Jacobson, M. Z. (2000), A physically-based treatment of elemental carbon optics: Implications for global direct forcing of aerosols, *Geophys. Res. Lett.*, *27*(2), 217–220, doi:10.1029/1999GL010968.

Jacobson, M. Z. (2001), Strong radiative heating due to the mixing state of black carbon in atmospheric aerosols, *Nature*, *409*, 695–697.

Jacobson, M. Z. (2002), Control of fossil-fuel particulate black carbon and organic matter, possibly the most effective method of slowing global warming, *J. Geophys. Res.*, *107*(D19), 4410, doi:10.1029/2001JD001376.

Jacobson, M. Z., R. P. Turco, E. J. Jensen, and O. B. Toon (1994), Modeling coagulation among particles of different composition and size, *Atmos. Environ.*, *28*, 1327–1338.

Kondo, Y., N. Oshima, M. Kajino, R. Mikami, N. Moteki, N. Takegawa, R. L. Verma, Y. Kajii, S. Kato, and A. Takami (2011a), Emissions of black carbon in East Asia estimated from observations at a remote site in the East China Sea, *J. Geophys. Res.*, *116*, D16201, doi:10.1029/2011JD015637.

Kondo, Y., L. Sahu, N. Moteki, F. Khan, N. Takegawa, X. Liu, M. Koike, and T. Miyakawa (2011b), Consistency and traceability of black carbon measurements made by laser-induced incandescence, thermal-optical transmittance, and filter-based photo-absorption techniques, *Aerosol Sci. Technol.*, *45*, 295–312.

Kondo, Y., H. Matsui, N. Moteki, L. Sahu, N. Takegawa, M. Kajino, Y. Zhao, M. J. Cubison, J. L. Jimenez, and S. Vay (2011c), Emissions of black carbon, organic, and inorganic aerosols from biomass burning in North America and Asia in 2008, *J. Geophys. Res.*, *116*, D08204, doi:10.1029/2010JD015152.

Kulmala, M., K. E. J. Lehtinen, and A. Laaksonen (2006), Cluster activation theory as an explanation of the linear dependence between formation rate of 3 nm particles and sulphuric acid concentration, *Atmos. Chem. Phys.*, *6*, 787–793.

Kuwata, M., Y. Kondo, and N. Takegawa (2009), Critical condensed mass for activation of black carbon as cloud condensation nuclei, *J. Geophys. Res.*, *114*, D20202, doi:10.1029/2009JD012086.

Lee, L. A., K. S. Carslaw, K. J. Pringle, and G. W. Mann (2012), Mapping the uncertainty in global CCN using emulation, *Atmos. Chem. Phys.*, *12*, 9739–9751.

Lee, L. A., K. J. Pringle, C. L. Reddington, G. W. Mann, P. Stier, D. V. Spracklen, J. R. Pierce, and K. S. Carslaw (2013), The magnitude and causes of uncertainty in global model simulations of cloud condensation nuclei, *Atmos. Chem. Phys.*, *13*, 8879–8914.

Liu, J., S. Fan, L. W. Horowitz, and H. Levy II (2011), Evaluation of factors controlling long-range transport of black carbon to the Arctic, *J. Geophys. Res.*, *116*, D04307, doi:10.1029/2010JD015145.

Matsui, H. (2016), Black carbon simulations using a size- and mixing-state-resolved three-dimensional model: 2. Aging timescale and its impact over East Asia, *J. Geophys. Res. Atmos.*, *121*, doi:10.1002/2015JD023999.

Matsui, H., M. Koike, Y. Kondo, N. Takegawa, A. Wiedensohler, J. D. Fast, and R. A. Zaveri (2011), Impact of new particle formation on the concentrations of aerosols and cloud condensation nuclei around Beijing, *J. Geophys. Res.*, *116*, D19208, doi:10.1029/2011JD016025.

Matsui, H., M. Koike, Y. Kondo, N. Moteki, J. D. Fast, and R. A. Zaveri (2013a), Development and validation of a black carbon mixing state resolved three-dimensional model: Aging processes and radiative impact, *J. Geophys. Res. Atmos.*, *118*, 2304–2326, doi:10.1029/2012JD018446.

Matsui, H., M. Koike, N. Takegawa, Y. Kondo, A. Takami, T. Takamura, S. Yoon, S.-W. Kim, H.-C. Lim, and J. D. Fast (2013b), Spatial and temporal variations of new particle formation in East Asia using an NPF-explicit WRF-chem model: North-south contrast in new particle formation frequency, *J. Geophys. Res. Atmos.*, *118*, 11,647–11,663, doi:10.1002/jgrd.50821.

Matsui, H., M. Koike, Y. Kondo, J. D. Fast, and M. Takigawa (2014a), Development of an aerosol microphysical module: Aerosol Two-dimensional bin module for foRmation and Aging Simulation (ATRAS), *Atmos. Chem. Phys.*, *14*, 10,315–10,331.

Matsui, H., M. Koike, Y. Kondo, A. Takami, J. D. Fast, Y. Kanaya, and M. Takigawa (2014b), Volatility basis-set approach simulation of organic aerosol formation in East Asia: Implications for anthropogenic–biogenic interaction and controllable amounts, *Atmos. Chem. Phys.*, *14*, 9513–9535.

Moteki, N., Y. Kondo, Y. Miyazaki, N. Takegawa, Y. Komazaki, G. Kurata, T. Shirai, D. R. Blake, T. Miyakawa, and M. Koike (2007), Evolution of mixing state of black carbon particles: Aircraft measurements over the western Pacific in March 2004, *Geophys. Res. Lett.*, *34*, L11803, doi:10.1029/2006GL028943.

Moteki, N., Y. Kondo, N. Oshima, N. Takegawa, M. Koike, K. Kita, H. Matsui, and M. Kajino (2012), Size dependence of wet removal of black carbon aerosols during transport from the boundary layer to the free troposphere, *Geophys. Res. Lett.*, *39*, L13802, doi:10.1029/2012GL052034.

Oshima, N., and M. Koike (2013), Development of a parameterization of black carbon aging for use in general circulation models, *Geosci. Model. Dev.*, *6*, 263–282.

Oshima, N., M. Koike, Y. Zhang, and Y. Kondo (2009), Aging of black carbon in outflow from anthropogenic sources using a mixing state resolved model: 2. Aerosol optical properties and cloud condensation nuclei activities, *J. Geophys. Res.*, *114*, D18202, doi:10.1029/2008JD011681.

Oshima, N., et al. (2012), Wet removal of black carbon in Asian outflow: Aerosol Radiative Forcing in East Asia (A-FORCE) aircraft campaign, *J. Geophys. Res.*, *117*, D03204, doi:10.1029/2011JD016552.

Petters, M. D., and S. M. Kreidenweis (2007), A single parameter representation of hygroscopic growth and cloud condensation nucleus activity, *Atmos. Chem. Phys.*, *7*, 1961–1971.

Ramanathan, V., and G. Carmichael (2008), Global and regional climate changes due to black carbon, *Nat. Geosci.*, *1*, 221–227.

Ramanathan, V., P. J. Crutzen, J. T. Kiehl, and D. Rosenfeld (2001), Aerosols, climate, and the hydrological cycle, *Science*, *294*(5549), 2119–2124.

Reddington, C. L., K. S. Carslaw, D. V. Spracklen, M. G. Frontoso, L. Collins, J. Merikanto, A. Minikin, T. Hamburger, H. Coe, and M. Kulmala (2011), Primary versus secondary contributions to particle number concentrations in the European boundary layer, *Atmos. Chem. Phys.*, *11*, 12,007–12,036.

Reddington, C. L., G. McMeeking, G. W. Mann, H. Coe, M. G. Frontoso, D. Liu, M. Flynn, D. V. Spracklen, and K. S. Carslaw (2013), The mass and number size distributions of black carbon aerosol over Europe, *Atmos. Chem. Phys.*, *13*, 4917–4939.

Riemer, N., H. Vogel, and B. Vogel (2004), Soot aging time scales in polluted regions during day and night, *Atmos. Chem. Phys.*, *4*, 1885–1893.

Riemer, N., M. West, R. A. Zaveri, and R. C. Easter (2010), Estimating soot aging time scales with a particle-resolved aerosol model, *J. Aerosol Sci.*, *41*, 143–158.

Seinfeld, J. H., and S. N. Pandis (2006), *Atmospheric Chemistry and Physics: From Air Pollution to Climate Change*, 2nd ed., John Wiley, New York.

Shiraiwa, M., Y. Kondo, N. Moteki, N. Takegawa, L. K. Sahu, A. Takami, S. Hatakeyama, S. Yonemura, and D. R. Blake (2008), Radiative impact of mixing state of black carbon aerosol in Asian outflow, *J. Geophys. Res.*, *113*, D24210, doi:10.1029/2008JD010546.

Shiraiwa, M., Y. Kondo, T. Iwamoto, and K. Kita (2010), Amplification of light absorption of black carbon by organic coating, *Aerosol Sci. Technol.*, *44*, 46–54.

Skamarock, W. C., J. B. Klemp, J. Dudhia, D. O. Gill, D. M. Barker, W. Wang, and J. G. Powers (2008), A description of the advanced research WRF version 3, *NCAR Tech. Note, NCAR/TN-475 + STR*, Natl. Cent. Atmos. Res., Boulder, Colo.

Stier, P., J. H. Seinfeld, S. Kinne, J. Feichter, and O. Boucher (2006), Impact of nonabsorbing anthropogenic aerosols on clear-sky atmospheric absorption, *J. Geophys. Res.*, *111*, D18201, doi:10.1029/2006JD007147.

Streets, D. G., et al. (2003), An inventory of gaseous and primary aerosol emissions in Asia in the year 2000, *J. Geophys. Res.*, *108*(D21), 8809, doi:10.1029/2002JD003093.

Takami, A., T. Miyoshi, A. Shimono, and S. Hatakeyama (2005), Chemical composition of fine aerosol measured by AMS at Fukue Island, Japan, during APEX period, *Atmos. Environ.*, *39*, 4913–4924.

Takami, A., T. Miyoshi, A. Shimono, N. Kaneyasu, S. Kato, Y. Kajii, and S. Hatakeyama (2007), Transport of anthropogenic aerosols from Asia and subsequent chemical transformation, *J. Geophys. Res.*, *112*, D22S31, doi:10.1029/2006JD008120.

van der Werf, G. R., J. T. Randerson, L. Giglio, G. J. Collatz, M. Mu, P. S. Kasibhatla, D. C. Morton, R. S. DeFries, Y. Jin, and T. T. van Leeuwen (2010), Global fire emissions and the contribution of deforestation, savanna, forest, agricultural, and peat fires (1997–2009), *Atmos. Chem. Phys.*, *10*, 11,707–11,735.

Wild, O., X. Zhu, and M. J. Prather (2000), Fast-J: Accurate simulation of in- and below-cloud photolysis in tropospheric chemical models, *J. Atmos. Chem.*, *37*, 245–282.

Zaveri, R. A., R. C. Easter, and A. S. Wexler (2005a), A new method for multicomponent activity coefficients of electrolytes in aqueous atmospheric aerosols, *J. Geophys. Res.*, *110*, D02201, doi:10.1029/2004JD004681.

Zaveri, R. A., R. C. Easter, and L. K. Peters (2005b), A computationally efficient Multicomponent Equilibrium Solver for Aerosols (MESA), *J. Geophys. Res.*, *110*, D24203, doi:10.1029/2004JD005618.

Zaveri, R. A., R. C. Easter, J. D. Fast, and L. K. Peters (2008), Model for Simulating Aerosol Interactions and Chemistry (MOSAIC), *J. Geophys. Res.*, *113*, D13204, doi:10.1029/2007JD008782.

Zaveri, R. A., J. C. Barnard, R. C. Easter, N. Riemer, and M. West (2010), Particle-resolved simulation of aerosol size, composition, mixing state, and the associated optical and cloud condensation nuclei activation properties in an evolving urban plume, *J. Geophys. Res.*, *115*, D17210, doi:10.1029/2009JD013616.